Distal immunization and systemic cytokines establish a transient immune alert state in the intestine

Authors: Yixuan Wu[1, 2], Jessica Y. Huang[1], Michael T. Conlon[1], Meera K. Shenoy[3], Jaime L. Chao[1], Ming Yao Chooi[2], Meghan A. Koch[3], Michael Y. Gerner[1]

[1]Department of Immunology, University of Washington, Seattle, USA

[2]Singapore Immunology Network, Agency for Science, Technology and Research, Singapore

[3]Basic Sciences Division, Fred Hutchinson Cancer Center, Seattle, USA

Abstract

Conventionally, immune responses are studied in the context of inflamed tissues and their corresponding draining lymph nodes (LNs). However, little is known about the effects of systemic inflammatory signals generated during local inflammation on distal tissues and non-draining LNs. Using a mouse model of cutaneous immunization, we found that systemic inflammatory stimuli triggered a rapid and selective distal response in the small intestine (SI) and the mesenteric LN (mesLN). This consisted of increased permeability of intestinal blood vessels and lymphatic drainage of bloodborne solutes into the mesLN, enhanced activation and migration of intestinal dendritic cells, as well as amplified T cell responses in the mesLNs to systemic but not orally derived antigens. Mechanistically, we found that the SI endothelial cells preferentially expressed molecules involved in TNFα signaling, and that TNFα blockade markedly diminished distal intestinal responses to cutaneous immunization. Together, these findings reveal that the intestinal immune system is rapidly and selectively activated in response to inflammatory cues regardless of their origin, thus identifying an additional layer of defence and enhanced surveillance of a key barrier organ at constant risk of pathogen encounter.

Introduction

Immunization or infection of peripheral tissues causes rapid activation of local innate sentinel cells, which produce cytokines and chemokines to alert neighbouring cells and recruit additional immune cells from the circulation (1, 2). Dendritic cells (DCs) within inflamed tissues capture locally available antigens, undergo maturation after sensing microbe-derived toll-like receptor (TLR) ligands or inflammatory cytokines, and migrate into local draining lymph nodes (LNs) to generate adaptive immune responses (3). Vaccine-derived antigens or microbes also drain directly into the local LNs via the lymphatics and induce responses by LN-resident DCs (4, 5). In this manner, vaccination or infection of peripheral tissues elicits localized response circuits within the affected tissues and their corresponding draining LNs, resulting in a compartmentalized host defence strategy. However, inflammatory cytokines also enter the circulation and can alert cells in distal organs (1, 6). For example, concurrent administration of a vaccine during viral infection generates elevated levels of type-I IFN, which induces an anti-viral state in cells across the entire body, even within organs highly distal to the vaccination site, and this limits further pathogen dissemination (7). On the other hand, overexuberant inflammation can promote immune pathology in distal sites, thereby necessitating a carefully balanced inflammatory response for optimized protection while maintaining organismal function (1, 8, 9).

To this end, it has previously been noted that systemic administration of certain TLR ligands induces DC maturation within both the spleen and the SI (10-12). While splenic responses are consistent with positioning of DCs in the bridging channels and direct access to TLR ligands in the circulation (13), the mechanisms driving DC responses in the SI are less clear, as these cells have limited access to circulating agonists (14, 15). It has been shown that a population of $CX3CR1^{+}$ myeloid cells within the SI lamina propria can sample systemic antigens (16), though the ability of these cells to migrate into the mesLNs has been debated (17, 18). Analogous innate responses to systemic TLR ligands have not been reported for other barrier organs, implying the existence of SI-specific responses to systemic stimuli.

In this regard, myeloid cells within the SI are highly specialized, comprising multiple intestine-specific DC and macrophage subsets which are essential for regulating the balance of tolerogenic and inflammatory responses to food-, commensal-, and pathogen-derived antigens (14, 15, 19). Recent studies have also demonstrated additional complexity in antigen presenting cells in the mesLN for promoting regulatory vs. effector T cell responses to intestinal antigens (20, 21). Moreover, blood and lymphatic endothelial cells within the SI are highly specialized to enable efficient nutrient absorption (22), and single-cell RNA sequencing (scRNA-seq) analysis of blood endothelial cells (BECs) across organs demonstrated divergent gene expression patterns and tissue-specific adaptations for the SI (23). The epithelial lining of the intestine is also highly sensitive to inflammatory cytokines, together suggesting that multiple hematopoietic and non-hematopoietic cell populations within the intestine have specialized tuning to inflammatory stimuli (24-26).

Here, we examined how distally generated inflammatory cues alter immune responses within the SI and the corresponding mesLNs. We find that immunization of a distal skin site with TLR agonists induces rapid and transient vascular endothelial and immune responses within the SI, but not in other distal barrier organs. These responses consist of rapid increases in SI blood vessel permeability and lymphatic drainage of diverse bloodborne macromolecules into the mesLN. We also find robust activation and migration of intestinal DCs

to the mesLN, as well as enhanced T cell activation to systemic antigens. Examination of published scRNA-seq data demonstrated that BECs in the SI have enhanced expression of multiple members of the TNFα signaling pathway, and blockade of TNFα during immunization inhibited the inflammatory response in the SI. Together, these findings suggest the existence of a mechanism for rapid intestinal alert which is generated even if the inflammatory signals originate in highly distal organs. This has important implications for understanding the regulation of intestinal vascular physiology during homeostasis and inflammation, generation of immune responses to systemic and gut-derived antigens, as well as general principles of immune surveillance and barrier defence in the SI.

Results

Enhanced activation and migration of intestinal DCs following distal cutaneous immunization

During immunization or infection, local innate cells, such as DCs, are rapidly activated within the inflamed barrier tissues as well as in the corresponding draining LNs. However, locally generated cytokines also enter the circulation and can potentially act upon cells in distal organs. To investigate whether innate cell activation occurs in distal LNs during a cutaneous inflammatory challenge, we immunized mice in the ear with Cytosine-phosphorothioate-guanine oligodeoxynucleotides (CpG), a TLR9 agonist which generates marked DC responses in local draining LNs (Fig. 1A) (27). Examination of responses using flow cytometry demonstrated a marked increase in DC cellularity in the mesLNs, which greatly surpassed that seen in skin-draining auricular LNs (aurLNs) and non-draining cutaneous inguinal LNs (ingLNs) (Fig. 1B). This increase in DC numbers in the mesLN was also associated with merging of the $CD11c^{HI}$ $MHC\text{-}II^{INT}$ and $CD11c^{INT}$ $MHC\text{-}II^{HI}$ DCs within 6h post-immunization (p.i.), making discrete gating of LN-resident and -migratory DC populations challenging (Fig. 1C). Instead, sub-gating of DCs based on additional phenotypic markers (Fig. 1D) revealed a significant increase in the proportion and cellularity of $CD103^{+}$ $CD11b^{+/-}$ and $CD103^{-}$ $CD11b^{+}$ DCs. Since $CD103^{+}$ $CD11b^{+}$ DCs normally reside in the intestinal lamina propria and migrate into mesLN following maturation, this suggested that distal cutaneous CpG administration elicits rapid migration of DCs from the intestine into the mesLN (Fig. 1E) (28). Consistent with this, changes in DC cellularity were associated with increased costimulatory molecule expression. As expected, increased CD80/86 expression was seen on DCs in skin-draining aurLNs (Fig. 1F-G) but not in non-draining ingLNs, suggesting minimal impact of skin immunization on distal cutaneous sites. In contrast, we observed marked CD86 and more modest CD80 upregulation by DCs in gut-draining mesLNs, which started as early as 3h p.i., peaked at 12h p.i., returned to baseline by 48h (Figs. 1F-H), and was particularly notable in $CD103^{+}$ $CD11b^{+/-}$ cells (Fig. 1I-J). Enhanced costimulatory molecule expression was also associated with a rapid spike in MHC-II expression for all DC populations, which returned to baseline within 10h p.i. (Fig. 1K).

We next analyzed DC distribution in mesLNs using histo-cytometry (29), and found an increased representation of $SIRP\alpha^{+}$ $CD103^{+}$ DCs as early as 6h after CpG immunization, which was consistent with our flow cytometry data (Supplemental Fig. 1A, 1B). Furthermore, we observed a significant increase in the number of $CD11c^{+}$ DCs within the deep T cell zone at 20h p.i. (Supplemental Fig. 1C), a time point corresponding to the peak of DC cellularity in the mesLN and consistent with the migration and repositioning of intestinal and LN-resident DCs into the T zone during maturation (Fig. 1B) (27). Together, these results indicate that in addition to local responses in the skin-draining LNs, distal cutaneous inflammation elicits robust activation and migration of intestinal DCs into the gut-draining mesLNs.

Distal inflammation induces transient intestinal endothelial permeability and activation of intestinal DCs

Myeloid cells in the SI have been previously shown to be intimately associated with local fenestrated blood vessels (BVs) (16). Increased DC responses in the mesLN after cutaneous immunization could thus reflect

their preferential ability to sample systemic signals and to migrate into the mesLNs after maturation. To study this, we imaged DCs in the SI 3h post distal skin immunization, while also labeling the BV-associated cells by intravenous (IV) administration of a fluorescently labeled CD11c antibody (30, 31). CD11c-IV antibody was administered 3h p.i. and SIs were isolated 30 minutes later to provide sufficient time for response induction and to enable robust cellular labeling, respectively (Fig. 2A). As expected, in naïve animals, we observed a dense aggregation of intestinal CD11c-expressing cells in the upper lamina propria (LP) of the villi, but relatively limited IV-labeling. In contrast, higher numbers of IV-labeled CD11c-expressing cells were observed near the basal lymphatic ducts (Fig. 2B), consistent with these cells starting to emigrate from the LP into the mesLN via the lymphatic lacteals.

We also visualized responses in the mesLNs 6h p.i., a time point at which DCs began to accumulate after cutaneous immunization (Fig. 1B). Here, we also observed markedly enhanced CD11c-IV labeling of cells after immunization, although surprisingly, this appeared to be highly enriched within the lymphatic subcapsular sinus (SCS) and not in the proximity of BVs (marked by CD105 staining) as would be expected for IV-administered probes (Fig. 2C). To investigate which DC populations were labeled with the IV probe, we analyzed the mesLNs from naïve and immunized mice via confocal microscopy and histo-cytometry. Further sub-gating and visualization of IV label-positive events demonstrated preferential enrichment of SIRPα^{+} CD103^{+} DCs, and positional mapping of these cells demonstrated predominant localization in the SCS regions (Supplemental Fig. 2A-B). In contrast to gut-draining mesLNs, IV-labeling in cutaneous draining aurLNs of naïve or immunized mice was limited and largely restricted to BV-proximal regions, as would be expected for IV-antibody staining (Supplemental Fig. 2C).

To further examine the kinetics of CD11c-IV-labeling in different LNs and across timepoints, we used flow cytometry. Enhanced IV-labeling of DCs was readily detected in the mesLNs but not in non-draining ingLNs and affected multiple DC subsets (Fig. 2D-F). Enhanced IV-labelling peaked ~4-6h p.i. and declined to levels below baseline ~12h p.i. In addition, we tested whether enhanced IV-labeling of DCs was restricted to CpG immunization or was more generalizable to other TLR agonists. We observed a spike in IV-labeling in mesLN DCs after subcutaneous administration of lipopolysaccharide (LPS) and polyinosinic:polycytidylic acid (p(I:C)) (Supplemental Fig. 2D-E), which was also associated with increased CD86 expression on DCs, together indicating that similar processes occur in response to multiple inflammatory agonists.

Increased IV-labeling of DCs both in the SI parenchyma and in the mesLN SCS after distal immunization suggested enhanced permeability of blood vessels in the SI and crossover of large bloodborne macromolecules, such as the CD11c-IV antibody, into the SI parenchyma and subsequent drainage into the mesLN. To test this possibility, we injected a large molecular weight FITC-dextran (500 kD) IV into either naïve or immunized animals (32). As expected, some FITC-dextran in the lymphatic sinuses was seen in naïve animals, consistent with a critical role for fluid transport in intestinal physiology and nutrient uptake. Importantly, we observed a significant increase in the deposition of FITC-dextran in the lymphatic sinuses of mesLNs 4h p.i., and this returned to below baseline levels at by 20h (Fig. 2G-H). In contrast, we did not find changes in dextran drainage in cutaneous draining aurLNs or non-draining ingLNs (Supplemental Fig. 2F), nor in lung-draining mediastinal LNs (medLNs) (Supplemental Fig. 2G), though the latter exhibited modestly

enhanced baseline drainage as compared to other tissues. Together, these data suggested that following immunization, there is a transient increase in vascular permeability and lymphatic drainage of large bloodborne macromolecules during inflammation, as well as the activation and migration of intestinal DCs into the mesLNs, and that this process preferentially occurs in the intestine and not other barrier tissues (i.e., skin and lung). To examine whether distal cutaneous inflammation also affected intestinal epithelial barrier integrity, we orally gavaged naïve or immunized animals with FITC-dextran and analyzed FITC fluorescence in the serum 2h later (Fig. 2I). As expected, we observed baseline uptake of FITC-dextran into the serum in control animals, consistent with normal absorption of nutrients via the intestinal epithelial lining (Fig. 2J). In contrast, cutaneous immunization reduced the amount of detectable FITC-dextran in the serum, suggesting that epithelial barrier integrity was preserved and, if anything, more restricted for gut luminal antigens after distal cutaneous immunization.

Heterogeneity of BEC populations across tissues, and involvement of the TNFα signaling in mediating intestinal responses to distal immunization

Selective increases in BV permeability in the SI suggested preferential intestinal BEC signaling in response to systemic factors generated during distal immunization. To examine this possibility, we performed unsupervised Gene Set Variation Analysis (GSVA) (33) using a published single-cell transcriptomic dataset of BECs isolated from various organs, including the SI, colon, kidney, lung, spleen, and soleus (23). Comparison with Molecular Signatures Database (MSigDB) hallmark gene sets revealed that BECs in different organs expressed unique pathway signatures, suggesting tissue-specific adaptations. In particular, BECs within the SI were highly enriched for multiple cytokine signaling pathways, including Type-I and -II interferons, interleukin-6 (IL-6), and TNFα (Fig. 3A). To identify genes in these cytokine pathways that were differentially expressed in SI BECs, we selected SI-expressed genes with a normalized gene expression across all six tissues (Fig. 3B). We found that out of these four, the TNFα pathway contained the highest number of differentially expressed genes, the majority of which were enriched in SI BECs compared to those from the other tissues.

This apparent sensitivity to TNFα was noteworthy, as during inflammation this cytokine can be rapidly released into the circulation by innate cells in both the skin and the draining LNs (34), and can directly promote endothelial permeability (35, 36) as well as induce DC activation (34, 37). Furthermore, TNFα, as well as other cytokines, was significantly elevated in draining LNs or serum samples after immunization with CpG, LPS, and poly(I:C), indicating possible involvement in systemic signaling (Fig. 3C-F). To directly test whether TNFα signaling promoted increased intestinal endothelial permeability and DC activation, we treated mice with anti-TNFα blocking or isotype control antibody 1h prior to cutaneous CpG administration. TNFα blockade significantly abrogated IV-labeling of DCs in the SI and mesLN (Fig. 4A-B), as well as drainage of IV-administered FITC-dextran to the mesLN 4h p.i. (Fig. 4C), indicating reduced vascular permeability and lymph drainage with anti-TNFα treatment. MesLN DCs from TNFα-blocked mice also exhibited a significantly reduced repositioning response, with fewer DCs seen within the T cell zone 24h p.i. (Fig. 4D). We also observed diminished CD86 expression and IV-labeling as quantified by flow cytometry

(Fig. 4E-F), together indicating a reduction in DC maturation and migration into mesLN in TNFα-blocked animals. Thus, TNFα signaling is at least in part responsible for increased intestinal endothelial permeability and lymphatic drainage, as well as DC maturation and migration into the mesLN following distal cutaneous immunization.

Cutaneous immunization potentiates adaptive immune responses to systemic antigens in mesLNs

We next examined whether distal alert of the intestinal immune system following cutaneous immunization could impacts the generation of T cell responses to systemic antigens in the mesLN. To test this, we adoptively transferred TCR transgenic, OVA-specific OT-I $CD8^+$ and OT-II $CD4^+$ T cells into naïve recipients, injected these mice with CpG in the distal skin, as well as administered OVA protein i.v. 3h later, and examined T cell responses across different LNs 4 days later. In order to eliminate potential contributions of cell recirculation through lymphoid organs and to retain activated T cells within the LNs in which they were primed, we also co-administered an S1P receptor inhibitor, FTY720, 2 and 3 days p.i. (Fig. 5A). As expected, we observed increased OT-I T cell cellularity in skin-draining aurLNs, consistent with enhanced inflammatory responses in local vaccination site-draining LNs (Fig. 5B). Notably, we also found significantly elevated cellularity and proliferation (by Ki67 expression) of OT-I T cells in the mesLNs, but not in non-draining cutaneous ingLNs (Fig. 5B-C). OT-I T cells in mesLNs of CpG-treated animals also selectively displayed reduced levels of CD62L and elevated levels of beta 7 integrin, indicating the generation of effector cells with altered homing potential and SI-trafficking capacity (Fig. 5D-E). Activated OT-I cells in the mesLNs also expressed CXCR3 and CD25, being consistent with the generation of effector cells, albeit the expression of these markers was not elevated with CpG administration in any of the LNs (Supplemental Fig. 3A-B). In contrast to $CD8^+$ T cell responses, $CD4^+$ OT-II cellularity and activation were largely unchanged across LNs after cutaneous CpG administration (Supplemental Fig. 3C-E), either reflecting preferential abilities of intestinal DCs to cross-present systemic antigens (16), or potential avidity differences between the TCR transgenic CD4 vs. CD8 T cells. A minor increase in the frequency of $CD25^+$ $CD62L^-$ activated OT-II cells in the mesLN was noted. Together, these data indicate that distal cutaneous inflammation promotes enhanced induction of CD8 T cell responses to systemic antigens in the mesLNs, but not in non-draining cutaneous LNs.

Finally, given that SI DCs are important for promoting oral tolerance to food-derived antigens through the generation of peripheral regulatory T cells (Tregs) in the mesLN (38, 39), we examined whether distal inflammation influences this process and can abrogate Treg induction. To test this, mice were adoptively transferred with OT-II T cells and fed OVA in drinking water for 7 days to induce Treg differentiation (40). Some mice also received cutaneous CpG injections every other day to trigger the intestinal alert response during OVA feeding (Fig. 5F). As expected, non-immunized animals developed a population of induced OVA-specific Tregs in the mesLNs as characterized by co-expression of CD25 and Foxp3 (Fig. 5G-H). Importantly, distal immunization with CpG did not alter Treg induction, nor did it induce enhanced expression of the transcription factor RORγt in the responding cells, indicating normal generation of Treg responses to orally administered antigens (Fig. 5H-J). Together, these data demonstrate that while distal immunization does

promote enhanced CD8 T cell activation to systemic proteins, it does not markedly alter CD4 T cell responses to either systemic or food-derived antigens.

Discussion

The intestine contains the highest microbial content of all the barrier surfaces, which includes both beneficial commensals as well as potentially harmful pathogens, thus necessitating rapid and effective strategies for barrier defence. Our findings indicate that the intestine is selectively tuned to respond to inflammatory stimuli even if these originate in highly distal tissues, and that equivalent responses are not seen in other barrier organs. Such selectivity appears at least in part driven by increased sensitivity of intestinal BECs to inflammatory cytokines, which during systemic inflammation appear to elicit enhanced blood vessel permeability and rapid lymphatic drainage of serum-associated macromolecules into the mesLNs. When coupled with rapid intestinal DC activation and migration into the mesLN, also likely potentiated by the same systemic cytokines, this enables effective delivery of information from the intestinal interstitium into the mesLN, thereby enhancing the generation of adaptive responses geared for intestinal protection. In addition to enhancing immune surveillance, the alert state could facilitate rapid delivery of additional immune mediators such as complement molecules into the SI for immediate anti-microbial function, as well as serum antibodies, which may provide additional barrier defence depending on previous pathogen exposure. Hence, we propose that this intestinal alert process represents a tissue-specific adaptation for enhanced immune detection and defence of a barrier organ under constant threat of bacterial translocation and infection.

The intestinal vasculature comprises specialized networks which collectively mediate diverse functions, most notably nutrient absorption during homeostatic conditions (41, 42). In contrast, during distal inflammation, the increased endothelial permeability of SI blood vessels could more selectively promote immune surveillance of the lamina propria instead of nutrient uptake. Moreover, we find that distal inflammation reduces the uptake of orally administered macromolecules, suggesting that luminal compartmentalization is actively enforced, if not enhanced, during this period. This could represent an additional layer of barrier defence, and the mechanisms driving this process could act directly downstream of inflammatory signaling in epithelial cells or be mediated indirectly by the perturbed interstitial fluid balance (22). Though TNFα signaling has been implicated in mouse models of intestinal inflammation, such as Dextran sodium sulfate (DSS)-induced colitis, to increase epithelial permeability by impairing tight junction integrity (43, 44), it is important to note that many of these models are also associated with actively disrupted barrier integrity and concurrent TNFα release, whereas the TNFα in our model is generated in response to distal inflammation in the absence of overt intestinal epithelial damage. Of relevance, it has been recently noted that chronic TNFα signaling during ileitis leads to the formation of tertiary lymphoid organs within the intestinal lymphatics which actively impede lymphatic drainage to the mesLN (45), indicating that while this cytokine has potentially beneficial effects via promoting transient alert in the SI, it can also lead to organ pathology in chronic inflammation settings.

The physical mechanisms by which TNFα (or other inflammatory mediators) preferentially regulate intestinal BEC responses during distal inflammation remain to be elucidated. One potential mechanism is via the fenestrae-forming plasmalemma vesicle-associated protein (PLVAP, aka PV1) which has been found on intestinal capillaries (23) and subcapsular sinus lymphatics in lymph nodes (48). Though functional knockouts of PLVAP have been well-characterized, it is unclear how its expression level or functional properties, and by extension vascular permeability (42, 49), are modulated during inflammatory conditions. Furthermore, it is

not known whether TNFα is the sole driver of endothelial cell permeability and DC activation, and multiple cytokines or other systemic factors could act in concert to activate either or both cell types (6). For example, cytokines such as type-I and -II IFNs were also elevated following cutaneous immunization and these may synergize with TNFα to drive increased vascular permeability in the SI (50, 51).

Like the intestine, the lung is a barrier organ whose function demands highly selective and regulated permeability at both the epithelial and endothelial layers (52). We did not detect major changes in lymphatic drainage into the medLN following distal immunization, indicating that lung endothelial permeability was not drastically altered under these experimental conditions. On a molecular level, our data demonstrate that endothelial cells across different tissues have non-equivalent expression of proteins in multiple cytokine signaling pathways and that this is likely responsible for the divergent responses. This likely reflects differential specialization of endothelial cells to serve their respective organs and the critical need of unperturbed pulmonary vasculature for optimal gas exchange and organismal function. Other structural factors such as the degree of capillary fenestration is also likely involved (46). Of note, sensitivity to cytokines other than TNFα, or to TLR agonists, has been shown to modulate pulmonary endothelial permeability in specific conditions, such as acute lung injury or acute respiratory distress syndrome (53-55).

Our data also indicate that the intestinal alert during distal inflammation promotes the generation of adaptive immune responses to systemic antigens, in particular for CD8 T cells, and that these mesLN-primed effector T cells express homing molecules for enhanced intestinal trafficking. While normally these responses would be geared towards gut-invasive pathogens, it is also possible that such distal activation in the mesLN could lead to aberrant immune responses against benign commensals, food antigens, or systemic antigens (56-58). Of note, in our hands, systemic inflammation did not result in detectable changes in TCR-transgenic CD4 T cell activation to either systemically or orally administered antigens, including normal induction of peripheral Tregs. While requiring additional functional testing, these findings suggest that there is a preferential effect of systemic inflammation on CD8 T cell immunity, and that induction of CD4 T cell oral tolerance remains intact. These data are also consistent with our findings that transient intestinal alert to distal inflammation occurs without concurrent disruption of epithelial permeability.

Finally, while providing a strategy for enhanced immunosurveillance of the intestine, it is possible that increased vascular permeability and drainage may also facilitate pathogen dissemination in some infection settings. Indeed, certain intestine-adapted pathogens such as *S. Typhimurium* have been shown to hijack vascular permeability to promote systemic dissemination via the hepatic portal vasculature (41, 47, 59). This may in turn activate the ‘intravascular firewall’ in the form of phagocytosis by Kupffer cells previously exposed to commensal-derived metabolites (60). Of note, while our studies focused on type-I inflammatory responses and early T cell activation in mesLNs, future work should also evaluate the impact of distal type-II inflammatory cytokines on intestinal alert responses, as this could play a role in atopic march development and induction of food allergies due to skin sensitization (61). On the other hand, the SI alert and distal adaptive immune responses could be potentially harnessed to develop multi-route (i.e. cutaneous plus mucosal) vaccination strategies to generate intestine-specific responses against oral pathogens (62). Altogether, the herein identified intestinal alert response to systemic cytokines may have broad implications, ranging from

roles in optimized intestinal barrier defence to involvement in unwanted inflammation and pathology, as well as in designing vaccines to enhance defence of the mucosal barrier.[

References

1. Turner MD, Nedjai B, Hurst T, Pennington DJ. Cytokines and chemokines: At the crossroads of cell signalling and inflammatory disease. Biochim Biophys Acta. 2014;1843(11):2563-82. Epub 20140602. doi: 10.1016/j.bbamcr.2014.05.014. PubMed PMID: 24892271.
2. Qi H, Kastenmüller W, Germain RN. Spatiotemporal basis of innate and adaptive immunity in secondary lymphoid tissue. Annu Rev Cell Dev Biol. 2014;30:141-67. Epub 20140808. doi: 10.1146/annurev-cellbio-100913-013254. PubMed PMID: 25150013.
3. Cabeza-Cabrerizo M, Cardoso A, Minutti CM, Pereira da Costa M, Reis ESC. Dendritic Cells Revisited. Annu Rev Immunol. 2021;39:131-66. Epub 20210122. doi: 10.1146/annurev-immunol-061020-053707. PubMed PMID: 33481643.
4. Gerner MY, Casey KA, Kastenmuller W, Germain RN. Dendritic cell and antigen dispersal landscapes regulate T cell immunity. Journal of Experimental Medicine. 2017;214(10):3105-22. doi: 10.1084/jem.20170335.
5. Huang JY, Lyons-Cohen MR, Gerner MY. Information flow in the spatiotemporal organization of immune responses. Immunol Rev. 2022;306(1):93-107. Epub 20211129. doi: 10.1111/imr.13046. PubMed PMID: 34845729; PubMed Central PMCID: PMC8837692.
6. Takahama M, Patil A, Richey G, Cipurko D, Johnson K, Carbonetto P, et al. A pairwise cytokine code explains the organism-wide response to sepsis. Nat Immunol. 2024;25(2):226-39. Epub 20240108. doi: 10.1038/s41590-023-01722-8. PubMed PMID: 38191855; PubMed Central PMCID: PMC10834370.
7. Kadoki M, Patil A, Thaiss CC, Brooks DJ, Pandey S, Deep D, et al. Organism-Level Analysis of Vaccination Reveals Networks of Protection across Tissues. Cell. 2017;171(2):398-413.e21. doi: 10.1016/j.cell.2017.08.024.
8. Barrat FJ, Crow MK, Ivashkiv LB. Interferon target-gene expression and epigenomic signatures in health and disease. Nat Immunol. 2019;20(12):1574-83. Epub 20191119. doi: 10.1038/s41590-019-0466-2. PubMed PMID: 31745335; PubMed Central PMCID: PMC7024546.
9. Crow MK, Olferiev M, Kirou KA. Type I Interferons in Autoimmune Disease. Annu Rev Pathol. 2019;14:369-93. Epub 20181017. doi: 10.1146/annurev-pathol-020117-043952. PubMed PMID: 30332560.
10. Turnbull EL, Yrlid U, Jenkins CD, MacPherson GG. Intestinal Dendritic Cell Subsets: Differential Effects of Systemic TLR4 Stimulation on Migratory Fate and Activation In Vivo. The Journal of Immunology. 2005;174(3):1374-84. doi: 10.4049/jimmunol.174.3.1374.
11. MacPherson GG, Jenkins CD, Stein MJ, Edwards C. Endotoxin-mediated dendritic cell release from the intestine. Characterization of released dendritic cells and TNF dependence. J Immunol. 1995;154(3):1317-22. PubMed PMID: 7822800.
12. Flores-Langarica A, Marshall JL, Hitchcock J, Cook C, Jobanputra J, Bobat S, et al. Systemic flagellin immunization stimulates mucosal CD103+ dendritic cells and drives Foxp3+ regulatory T cell and IgA responses in the mesenteric lymph node. J Immunol. 2012;189(12):5745-54. Epub 20121114. doi: 10.4049/jimmunol.1202283. PubMed PMID: 23152564.
13. Eisenbarth SC. Dendritic cell subsets in T cell programming: location dictates function. Nat Rev Immunol. 2019;19(2):89-103. doi: 10.1038/s41577-018-0088-1. PubMed PMID: 30464294; PubMed Central PMCID: PMC7755085.
14. Stagg AJ. Intestinal Dendritic Cells in Health and Gut Inflammation. Front Immunol. 2018;9:2883. Epub 20181206. doi: 10.3389/fimmu.2018.02883. PubMed PMID: 30574151; PubMed Central PMCID: PMC6291504.
15. Coombes JL, Powrie F. Dendritic cells in intestinal immune regulation. Nat Rev Immunol. 2008;8(6):435-46. doi: 10.1038/nri2335. PubMed PMID: 18500229; PubMed Central PMCID: PMC2674208.
16. Chang SY, Song JH, Guleng B, Cotoner CA, Arihiro S, Zhao Y, et al. Circulatory antigen processing by mucosal dendritic cells controls CD8(+) T cell activation. Immunity. 2013;38(1):153-65. Epub 20121213. doi: 10.1016/j.immuni.2012.09.018. PubMed PMID: 23246312; PubMed Central PMCID: PMC3858856.
17. Schulz O, Jaensson E, Persson EK, Liu X, Worbs T, Agace WW, et al. Intestinal CD103+, but not CX3CR1+, antigen sampling cells migrate in lymph and serve classical dendritic cell functions. J Exp Med. 2009;206(13):3101-14. Epub 20091214. doi: 10.1084/jem.20091925. PubMed PMID: 20008524; PubMed Central PMCID: PMC2806467.
18. Diehl GE, Longman RS, Zhang JX, Breart B, Galan C, Cuesta A, et al. Microbiota restricts trafficking of bacteria to mesenteric lymph nodes by CX(3)CR1(hi) cells. Nature. 2013;494(7435):116-20. Epub 20130113. doi: 10.1038/nature11809. PubMed PMID: 23334413; PubMed Central PMCID: PMC3711636.
19. Esterházy D, Loschko J, London M, Jove V, Oliveira TY, Mucida D. Classical dendritic cells are required for dietary antigen–mediated induction of peripheral Treg cells and tolerance. Nature Immunology. 2016;17(5):545-55. doi: 10.1038/ni.3408.

20. Kedmi R, Najar TA, Mesa KR, Grayson A, Kroehling L, Hao Y, et al. A RORγt+ cell instructs gut microbiota-specific Treg cell differentiation. Nature. 2022:1-7. doi: 10.1038/s41586-022-05089-y.
21. Akagbosu B, Tayyebi Z, Shibu G, Paucar Iza YA, Deep D, Parisotto YF, et al. Novel antigen-presenting cell imparts T_{reg}-dependent tolerance to gut microbiota. Nature. 2022;610(7933):752-60. Epub 20220907. doi: 10.1038/s41586-022-05309-5. PubMed PMID: 36070798; PubMed Central PMCID: PMC9605865.
22. Kvietys PR, Granger DN. Role of intestinal lymphatics in interstitial volume regulation and transmucosal water transport. Ann N Y Acad Sci. 2010;1207 Suppl 1(Suppl 1):E29-43. doi: 10.1111/j.1749-6632.2010.05709.x. PubMed PMID: 20961304; PubMed Central PMCID: PMC2966032.
23. Kalucka J, de Rooij LPMH, Goveia J, Rohlenova K, Dumas SJ, Meta E, et al. Single-Cell Transcriptome Atlas of Murine Endothelial Cells. Cell. 2020;180(4):764-79.e20. doi: 10.1016/j.cell.2020.01.015.
24. Ma TY, Boivin MA, Ye D, Pedram A, Said HM. Mechanism of TNF-{alpha} modulation of Caco-2 intestinal epithelial tight junction barrier: role of myosin light-chain kinase protein expression. Am J Physiol Gastrointest Liver Physiol. 2005;288(3):G422-30. doi: 10.1152/ajpgi.00412.2004. PubMed PMID: 15701621.
25. Madara JL, Stafford J. Interferon-gamma directly affects barrier function of cultured intestinal epithelial monolayers. J Clin Invest. 1989;83(2):724-7. doi: 10.1172/JCI113938. PubMed PMID: 2492310; PubMed Central PMCID: PMC303735.
26. Al-Sadi RM, Ma TY. IL-1beta causes an increase in intestinal epithelial tight junction permeability. J Immunol. 2007;178(7):4641-9. doi: 10.4049/jimmunol.178.7.4641. PubMed PMID: 17372023; PubMed Central PMCID: PMC3724221.
27. Leal JM, Huang JY, Kohli K, Stoltzfus C, Lyons-Cohen MR, Olin BE, et al. Innate cell microenvironments in lymph nodes shape the generation of T cell responses during type I inflammation. Science Immunology. 2021;6(56):eabb9435. doi: 10.1126/sciimmunol.abb9435.
28. Stagg AJ. Intestinal Dendritic Cells in Health and Gut Inflammation. Frontiers in Immunology. 2018;9:2883. doi: 10.3389/fimmu.2018.02883.
29. Gerner Michael Y, Kastenmuller W, Ifrim I, Kabat J, Germain Ronald N. Histo-Cytometry: A Method for Highly Multiplex Quantitative Tissue Imaging Analysis Applied to Dendritic Cell Subset Microanatomy in Lymph Nodes. Immunity. 2012;37(2):364-76. doi: 10.1016/j.immuni.2012.07.011.
30. Vollmann EH, Rattay K, Barreiro O, Thiriot A, Fuhlbrigge RA, Vrbanac V, et al. Specialized transendothelial dendritic cells mediate thymic T-cell selection against blood-borne macromolecules. Nat Commun. 2021;12(1):6230. Epub 20211028. doi: 10.1038/s41467-021-26446-x. PubMed PMID: 34711828; PubMed Central PMCID: PMC8553756.
31. Ugur M, Labios RJ, Fenton C, Knöpper K, Jobin K, Imdahl F, et al. Lymph node medulla regulates the spatiotemporal unfolding of resident dendritic cell networks. Immunity. 2023;56(8):1778-93.e10. Epub 20230717. doi: 10.1016/j.immuni.2023.06.020. PubMed PMID: 37463581; PubMed Central PMCID: PMC10433941.
32. Masedunskas A, Weigert R. Intravital two-photon microscopy for studying the uptake and trafficking of fluorescently conjugated molecules in live rodents. Traffic. 2008;9(10):1801-10. Epub 20080718. doi: 10.1111/j.1600-0854.2008.00798.x. PubMed PMID: 18647170; PubMed Central PMCID: PMC2711521.
33. Hänzelmann S, Castelo R, Guinney J. GSVA: gene set variation analysis for microarray and RNA-seq data. BMC Bioinformatics. 2013;14:7. Epub 20130116. doi: 10.1186/1471-2105-14-7. PubMed PMID: 23323831; PubMed Central PMCID: PMC3618321.
34. Dudeck J, Kotrba J, Immler R, Hoffmann A, Voss M, Alexaki VI, et al. Directional mast cell degranulation of tumor necrosis factor into blood vessels primes neutrophil extravasation. Immunity. 2021;54(3):468-83.e5. doi: 10.1016/j.immuni.2020.12.017.
35. Jeong J-H, Kim K, Lim D, Kim K-H, Kim H-S, Lee S, et al. Microvasculature remodeling in the mouse lower gut during inflammaging. Scientific Reports. 2017;7(1):1-8. doi: 10.1038/srep39848.
36. Girbl T, Lenn T, Perez L, Rolas L, Barkaway A, Thiriot A, et al. Distinct Compartmentalization of the Chemokines CXCL1 and CXCL2 and the Atypical Receptor ACKR1 Determine Discrete Stages of Neutrophil Diapedesis. Immunity. 2018;49(6):1062-76.e6. doi: 10.1016/j.immuni.2018.09.018.
37. Yrlid U, Milling SWF, Miller JL, Cartland S, Jenkins CD, MacPherson GG. Regulation of Intestinal Dendritic Cell Migration and Activation by Plasmacytoid Dendritic Cells, TNF-α and Type 1 IFNs after Feeding a TLR7/8 Ligand. The Journal of Immunology. 2006;176(9):5205-12. doi: 10.4049/jimmunol.176.9.5205.
38. Sun CM, Hall JA, Blank RB, Bouladoux N, Oukka M, Mora JR, et al. Small intestine lamina propria dendritic cells promote de novo generation of Foxp3 T reg cells via retinoic acid. J Exp Med. 2007;204(8):1775-85. Epub 20070709. doi: 10.1084/jem.20070602. PubMed PMID: 17620362; PubMed Central PMCID: PMC2118682.

39. Coombes JL, Siddiqui KRR, Arancibia-Cárcamo CV, Hall J, Sun C-M, Belkaid Y, et al. A functionally specialized population of mucosal CD103+ DCs induces Foxp3+ regulatory T cells via a TGF-β– and retinoic acid–dependent mechanism. Journal of Experimental Medicine. 2007;204(8):1757-64. doi: 10.1084/jem.20070590.
40. Hill JA, Hall JA, Sun C-M, Cai Q, Ghyselinck N, Chambon P, et al. Retinoic Acid Enhances Foxp3 Induction Indirectly by Relieving Inhibition from CD4+CD44hi Cells. Immunity. 2008;29(5):758-70. doi: 10.1016/j.immuni.2008.09.018.
41. Brescia P, Rescigno M. The gut vascular barrier: a new player in the gut-liver-brain axis. Trends Mol Med. 2021;27(9):844-55. Epub 20210703. doi: 10.1016/j.molmed.2021.06.007. PubMed PMID: 34229973.
42. Bernier-Latmani J, González-Loyola A, Petrova TV. Mechanisms and functions of intestinal vascular specialization. J Exp Med. 2024;221(1). Epub 20231205. doi: 10.1084/jem.20222008. PubMed PMID: 38051275; PubMed Central PMCID: PMC10697212.
43. Odenwald MA, Turner JR. The intestinal epithelial barrier: a therapeutic target? Nat Rev Gastroenterol Hepatol. 2017;14(1):9-21. Epub 20161116. doi: 10.1038/nrgastro.2016.169. PubMed PMID: 27848962; PubMed Central PMCID: PMC5554468.
44. Ahmad R, Sorrell MF, Batra SK, Dhawan P, Singh AB. Gut permeability and mucosal inflammation: bad, good or context dependent. Mucosal Immunol. 2017;10(2):307-17. Epub 20170125. doi: 10.1038/mi.2016.128. PubMed PMID: 28120842; PubMed Central PMCID: PMC6171348.
45. Czepielewski RS, Erlich EC, Onufer EJ, Young S, Saunders BT, Han Y-H, et al. Ileitis-associated tertiary lymphoid organs arise at lymphatic valves and impede mesenteric lymph flow in response to tumor necrosis factor. Immunity. 2021;54(12):2795-811.e9. doi: 10.1016/j.immuni.2021.10.003.
46. Stan RV, Kubitza M, Palade GE. PV-1 is a component of the fenestral and stomatal diaphragms in fenestrated endothelia. Proc Natl Acad Sci U S A. 1999;96(23):13203-7. doi: 10.1073/pnas.96.23.13203. PubMed PMID: 10557298; PubMed Central PMCID: PMC23925.
47. Spadoni I, Zagato E, Bertocchi A, Paolinelli R, Hot E, Sabatino AD, et al. A gut-vascular barrier controls the systemic dissemination of bacteria. 2015:6.
48. Rantakari P, Auvinen K, Jäppinen N, Kapraali M, Valtonen J, Karikoski M, et al. The endothelial protein PLVAP in lymphatics controls the entry of lymphocytes and antigens into lymph nodes. Nature Immunology. 2015;16(4):386-96. doi: 10.1038/ni.3101.
49. Chang TH, Hsieh FL, Gu X, Smallwood PM, Kavran JM, Gabelli SB, et al. Structural insights into plasmalemma vesicle-associated protein (PLVAP): Implications for vascular endothelial diaphragms and fenestrae. Proc Natl Acad Sci U S A. 2023;120(14):e2221103120. Epub 20230330. doi: 10.1073/pnas.2221103120. PubMed PMID: 36996108; PubMed Central PMCID: PMC10083539.
50. Langer V, Vivi E, Regensburger D, Winkler TH, Waldner MJ, Rath T, et al. IFN-γ drives inflammatory bowel disease pathogenesis through VE-cadherin-directed vascular barrier disruption. J Clin Invest. 2019;129(11):4691-707. doi: 10.1172/JCI124884. PubMed PMID: 31566580; PubMed Central PMCID: PMC6819119.
51. Labarta-Bajo L, Nilsen SP, Humphrey G, Schwartz T, Sanders K, Swafford A, et al. Type I IFNs and CD8 T cells increase intestinal barrier permeability after chronic viral infection. J Exp Med. 2020;217(12). doi: 10.1084/jem.20192276. PubMed PMID: 32880630; PubMed Central PMCID: PMC7953738.
52. Lucas R, Hadizamani Y, Enkhbaatar P, Csanyi G, Caldwell RW, Hundsberger H, et al. Dichotomous Role of Tumor Necrosis Factor in Pulmonary Barrier Function and Alveolar Fluid Clearance. Front Physiol. 2021;12:793251. Epub 20220221. doi: 10.3389/fphys.2021.793251. PubMed PMID: 35264975; PubMed Central PMCID: PMC8899333.
53. Ganter MT, Roux J, Miyazawa B, Howard M, Frank JA, Su G, et al. Interleukin-1beta causes acute lung injury via alphavbeta5 and alphavbeta6 integrin-dependent mechanisms. Circ Res. 2008;102(7):804-12. Epub 20080214. doi: 10.1161/CIRCRESAHA.107.161067. PubMed PMID: 18276918; PubMed Central PMCID: PMC2739091.
54. Jiao H, Zhang Y, Yan Z, Wang ZG, Liu G, Minshall RD, et al. Caveolin-1 Tyr14 phosphorylation induces interaction with TLR4 in endothelial cells and mediates MyD88-dependent signaling and sepsis-induced lung inflammation. J Immunol. 2013;191(12):6191-9. Epub 20131115. doi: 10.4049/jimmunol.1300873. PubMed PMID: 24244013; PubMed Central PMCID: PMC3874812.
55. Vassiliou AG, Kotanidou A, Dimopoulou I, Orfanos SE. Endothelial Damage in Acute Respiratory Distress Syndrome. Int J Mol Sci. 2020;21(22). Epub 20201120. doi: 10.3390/ijms21228793. PubMed PMID: 33233715; PubMed Central PMCID: PMC7699909.
56. Hand TW, Dos Santos LM, Bouladoux N, Molloy MJ, Pagán AJ, Pepper M, et al. Acute gastrointestinal infection induces long-lived microbiota-specific T cell responses. Science. 2012;337(6101):1553-6. Epub 20120823. doi: 10.1126/science.1220961. PubMed PMID: 22923434; PubMed Central PMCID: PMC3784339.

57. Belkaid Y, Harrison OJ. Homeostatic Immunity and the Microbiota. Immunity. 2017;46(4):562-76. doi: 10.1016/j.immuni.2017.04.008. PubMed PMID: 28423337; PubMed Central PMCID: PMC5604871.
58. Yu W, Freeland DMH, Nadeau KC. Food allergy: immune mechanisms, diagnosis and immunotherapy. Nature Reviews Immunology. 2016;16(12):751-65. doi: 10.1038/nri.2016.111.
59. Spadoni I, Pietrelli A, Pesole G, Rescigno M. Gene expression profile of endothelial cells during perturbation of the gut vascular barrier. Gut Microbes. 2016;7(6):540-8. Epub 20161010. doi: 10.1080/19490976.2016.1239681. PubMed PMID: 27723418; PubMed Central PMCID: PMC5153614.
60. McDonald B, Zucoloto AZ, Yu IL, Burkhard R, Brown K, Geuking MB, et al. Programing of an Intravascular Immune Firewall by the Gut Microbiota Protects against Pathogen Dissemination during Infection. Cell Host Microbe. 2020;28(5):660-8.e4. Epub 20200817. doi: 10.1016/j.chom.2020.07.014. PubMed PMID: 32810440.
61. Han H, Roan F, Ziegler SF. The atopic march: current insights into skin barrier dysfunction and epithelial cell-derived cytokines. Immunol Rev. 2017;278(1):116-30. doi: 10.1111/imr.12546. PubMed PMID: 28658558; PubMed Central PMCID: PMC5492959.
62. Bošnjak B, Odak I, Barros-Martins J, Sandrock I, Hammerschmidt SI, Permanyer M, et al. Intranasal Delivery of MVA Vector Vaccine Induces Effective Pulmonary Immunity Against SARS-CoV-2 in Rodents. Front Immunol. 2021;12:772240. Epub 20211111. doi: 10.3389/fimmu.2021.772240. PubMed PMID: 34858430; PubMed Central PMCID: PMC8632543.
63. Gerner Michael Y, Torabi-Parizi P, Germain Ronald N. Strategically Localized Dendritic Cells Promote Rapid T Cell Responses to Lymph-Borne Particulate Antigens. Immunity. 2015;42(1):172-85. doi: 10.1016/j.immuni.2014.12.024.

Methods

Animals

C57BL/6J male mice were obtained from The Jackson Laboratory. CD45.1+ C57BL/6-Tg(TcraTcrb)1100Mjb/J (OT-I), CD45.1$^+$ B6.Cg-Tg(TcraTcrb)425Cbn/J (OT-II), and B6.SJL-PtprcaPepcb/BoyCrl (CD45.1$^+$) were obtained either from a donating investigator (P. J. Fink, University of Washington) or Charles River. All mice were kept in specific pathogen–free conditions at an Association for Assessment and Accreditation of Laboratory Animal Care–accredited animal facility at the University of Washington, South Lake Union campus. All procedures were approved by the University of Washington Institutional Animal Care and Use Committee.

Immunizations and Treatments

All experiments were performed in male animals. For immunization studies, the following amounts of adjuvants were injected per site: 20 µg of CpG ODN 1668 (AdipoGen), 20 µg of LPS from *E. coli* O111:B4 (Sigma-Aldrich), or 20 µg of poly(I:C) (Amersham) diluted 1:2 with PBS. All adjuvants were injected either intradermally in the ear pinnae, or the front footpads (targeting the auricular or brachial LNs respectively).

For intravenous labeling studies, 3 µg of CD11c-PE antibody (clone HL3, BD Pharmingen) and/or 0.5 mg of FITC-Dextran conjugate (500 kD, Invitrogen) were diluted in PBS (up to a final volume of 200 µL per mouse) and injected retro-orbitally 30 mins prior to euthanasia.

For *in vivo* antibody blocking studies, 0.5 mg of *InVivo*Mab anti-TNFα antibody (clone XT3.11, BioXCell) or *InVivo*Mab IgG1 isotype control (clone HRPN, BioXCell) were diluted in PBS (up to a final volume of 200 µL per mouse) and injected intraperitoneally 1h prior to immunization with adjuvant.

For studies utilizing adoptive transfers, naïve CD45.1$^+$ OT-I or OT-II T cells were isolated from LNs and spleens using their respective naïve CD8$^+$ or CD4$^+$ T cell isolation kits (Miltenyi Biotec). Purity was checked via flow cytometry. The indicated number of cells was resuspended in PBS (up to a final volume of 200 µL per mouse) and transferred into CD45.2$^+$ C57BL/6J recipients via intravenous retro-orbital injection.

For studies testing the response to systemic antigen, 10 µg of endotoxin-free OVA (InvivoGen) was diluted in PBS (up to a final volume of 200 µL per mouse) and administered via intravenous retro-orbital injection 3h

following immunization with adjuvant. In some of these studies, FTY720 was diluted to a final concentration of 0.2 mg/mL in PBS, vortexed for 10-15 mins, and injected intraperitoneally at a dose of 1 mg/kg body weight.

For oral tolerance studies, Grade II albumin from chicken egg white (Sigma-Aldrich) was resuspended in water at 1.5% concentration and administered via drinking water for 7 days.

Confocal Microscopy and Histo-cytometry

Isolated tissues were fixed overnight at 4ºC in Cytofix (BD) diluted 1:3 with PBS, cryoprotected in 30% sucrose for 8-24h, embedded in O.C.T. compound (Tissue-Tek), and stored at -80ºC. Tissues were sectioned on a Microm HM550 cryostat (Thermo Scientific) at 20 µm thickness, then imaged on a Leica SP8 confocal microscope using a 20x 0.7 NA oil-immersion objective as previously described (27). Compensation was performed on raw images using LAS-X (Leica), followed by image visualization and analysis using Imaris (Bitplane). Spot object creation and T cell zone demarcation were performed in Imaris as previously described (27).

For histo-cytometry analysis, CD11c-expressing cell objects were generated in Imaris and data on marker intensity and object positioning was exported for additional quantification and visualization in FlowJo (BD Biosciences), as previously described (27, 29, 63).

Flow Cytometry

For myeloid cell studies, LNs were physically disrupted using forceps and enzymatically digested with an enzymatic cocktail consisting of Collagenase P (0.2 mg/mL in HBSS, Sigma-Aldrich), Dispase II (0.8 mg/mL, Sigma-Aldrich), DNase I (0.1 mg/mL, Sigma-Aldrich), and FCS (1%, Corning) in RPMI 1640 medium (Fisher Scientific). For T cell studies, LNs were physically disrupted using forceps and digested with Collagenase D (1.08 mg/mL, Sigma-Aldrich). Data were acquired on a Cytek Aurora (Cytek Biosciences) or an LSR-II (BD Biosciences) flow cytometer and analyzed using FlowJo software.

Intestinal Permeability Assay

Intestinal epithelial permeability was assessed via a FITC-dextran leakage assay. 15-week-old littermate mice were fasted for 4h, followed by oral gavage with 10 mg of 4 kD FITC-dextran or PBS (as a negative control). Mice were then anesthetized and injected with CpG or PBS in both ears. 2h later, mice were euthanized. Blood was harvested via cardiac puncture and centrifuged to obtain serum. FITC-dextran levels in serum (488 nm excitation, 516 nm emission) were measured on a microplate reader, and FITC-dextran concentration was determined using a standard curve.

Antibodies and Staining Reagents

Antibodies used for staining tissue sections for confocal microscopy and/or cells for flow cytometry include:

CD3 (clone 17A2; Biolegend, BD), CD4 (clone RM4-5; BD), CD8 (clone 53-6.7; Biolegend), CD11b (clone M1/70; Biolegend), CD11c (clone HL3; BD), CD11c (clone N4/18; BD), CD25 (PC61.5; Invitrogen), CD44 (clone IM7; Biolegend), CD45.1 (clone A20; Biolegend), CD45.2 (clone 104; Biolegend, BD), CD62L (clone MEL-14; BD), CD64 (clone X54-5/7.1; Biolegend), CD80 (clone 16-1A1; BD), CD86 (clone GL1; Biolegend), CD103 (clone M290; BD), CD105 (REA1058; Miltenyi Biotec), B220 (clone RA3-6B2; Biolegend), Clec9a (AF6776; R&D), Collagenase IV (clone N120-6586; Novus Bio), Foxp3 (clone FJK-16s; eBioscience), Integrin β7 (clone FIB504; eBioscience), Ki67 (B56; BD), Ly6G (clone 1A8; Biolegend), Lyve1 (clone ALY7; Invitrogen), MECA-79 (clone MECA-79; Biolegend), MHC-II (clone M5/114.15.2; Biolegend), NK1.1 (clone PK136; Biolegend), Rorgt (clone Q31378; BD), SIRPα (clone P84; Biolegend), Ter119 (clone ter-119; Biolegend), XCR1 (clone ZET; Biolegend).

Analysis of Publicly Available Endothelial Cell Data

Single-cell RNA sequencing data of endothelial subsets across six organs (SI, colon, lung, spleen, kidney, and soleus) were obtained from a published data set (23) and processed to obtain transcriptomic profiles of average log-transformed normalized gene expression. GSVA (33) enrichment was then performed on these transcriptomic profiles in comparison to the mSigDB Hallmark and Pathway Interaction Database (http://pid.nci.nih.gov) gene sets to identify key signaling pathways that were differentially enriched in endothelial populations from these organs.

Serum and Lymph Node Cytokine Analysis

To quantify cytokine levels, mice were immunized in both ear pinnae and forepaws with CpG (20 ug/site), LPS (10 ug/site), or poly(I:C) (20 ug/site). 6h later, draining LNs and sera were harvested. LNs from each mouse were pooled, lysed using a Precellys CK14 Lysing Kit (Berin Corp) in 1X Pierce Protease Inhibitor (Thermo Scientific), and concentrated using 30K Amicon filters (Millipore). Samples were then processed with a LEGENDPlex Mouse Inflammation Panel kit (Biolegend) according to the manufacturer's instructions and analyzed by flow cytometry on a BD LSRII (BD Biosciences). Data were then analyzed using LEGENDplex software (Biolegend).

Statistics

Statistical analysis was performed using GraphPad Prism software. For studies involving side-by-side groups, unpaired t-test or one-way ANOVA was used together with the Benjamini, Krieger, and Yekutieli False Discovery Rate correction for multiple comparisons. For infection studies, the Kruskal-Wallis test was used together with the Benjamini-Hochberg False Discovery Rate correction for multiple comparisons. In bar graphs for all figures, error bars represent the SD. For time course data, * = $P < 0.05$ and # = $P < 0.0001$ and show statistical significance between the indicated time point and the naïve control group. In all figures, data points represent either pooled (auricular, brachial LNs) or independent (mesLN) tissues, and a minimum of 3 mice were used per group.

Data availability

Values for all data points in graphs are reported in the Supporting Data Values file.

Author contributions

Y.W. designed, performed, and analyzed most of the experiments, and wrote the manuscript. J.Y.H., M.T.C., and J.L.C. performed and analyzed some immunization, adoptive transfer, and LEGENDplex experiments,

592 respectively. M.K.S. designed, performed and analyzed the oral gavage experiments. M.Y.C. analyzed the
593 endothelial cell RNA-Seq data. M.A.K. provided scientific and material support. M.Y.G. designed and
594 supervised the overall research and wrote the manuscript.

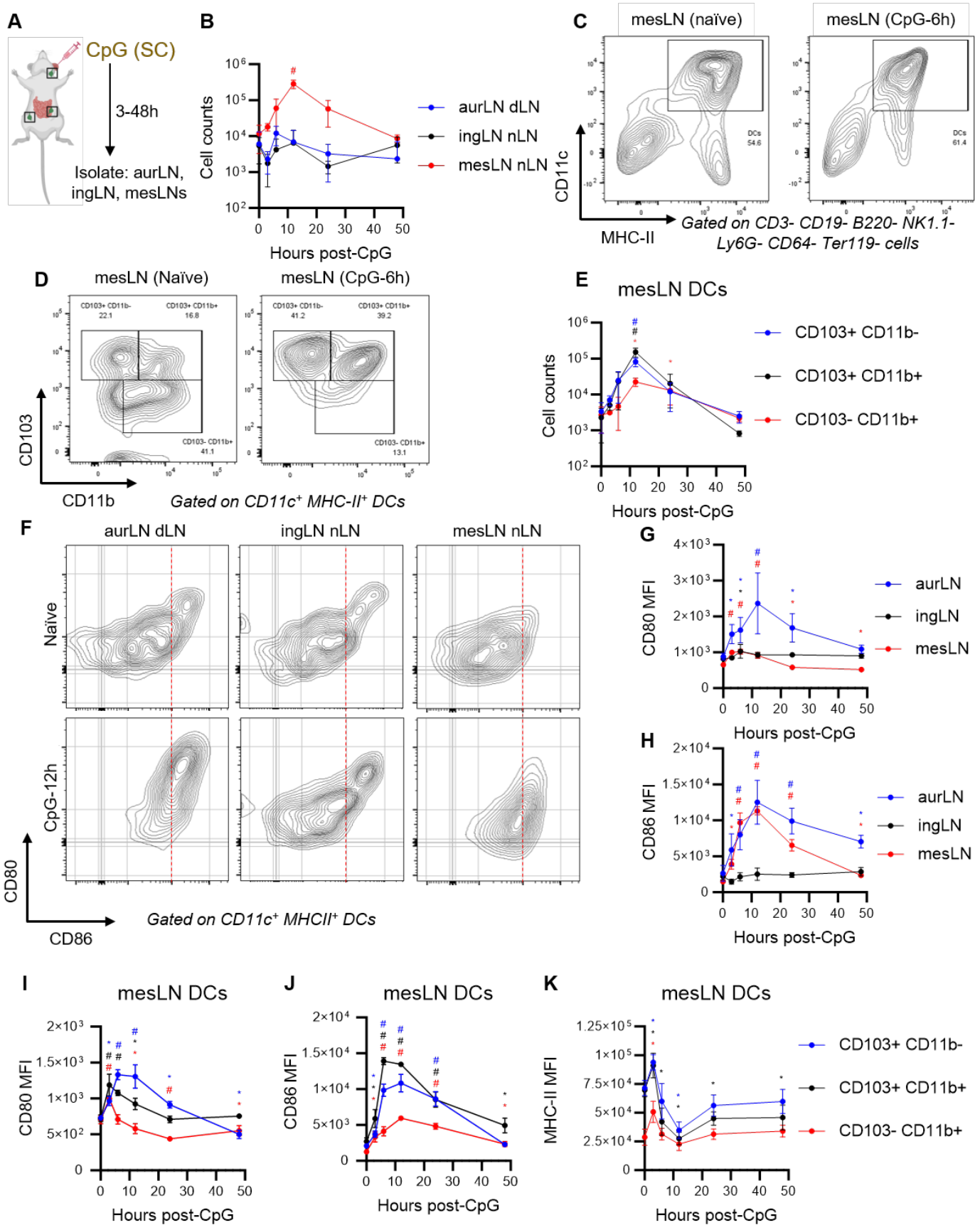

Figure 1. Enhanced activation and migration of intestinal DCs following distal cutaneous immunization (A) C57BL6/J mice were injected subcutaneously (SC) in both ears with CpG or left untreated and indicated LNs were harvested at indicated time points for analysis. **(B)** Time course of DC cellularity for DCs from various LNs post-immunization (p.i.) (*n* = 3-4 mice). **(C-D)** Representative flow cytometry plots showing gating of CD11c$^+$ MHC-II$^+$ mesLN DCs (C) and expression of CD103 and CD11b on the gated subset (D) at 6h p.i. **(E)** Time course of cellularity for the indicated mesLN DC subsets p.i. (*n* = 3-4 mice). **(F)**

Representative flow cytometry plots showing CD80 and CD86 expression on DCs in LNs at 12h p.i. **(G-H)** Time course of CD80 (G) and CD86 (H) expression on DCs from various LNs p.i. (*n* = 3-4 mice). **(I-K)** Time course of CD80 (I), CD86 (J), and MHC-II (K) expression on the indicated mesLN DC subsets p.i. (*n* = 3-4 mice). Data in (B), (C), (G), (H), (I), (J), and (K) were analyzed via one-way ANOVA with Benjamini, Krieger, and Yekutieli correction for multiple comparisons. * = $P < 0.05$ and # = $P < 0.0001$, and show statistical significance between the indicated time point and the naïve control group. Data are representative of at least two independent experiments. (A) was created on Biorender.com.

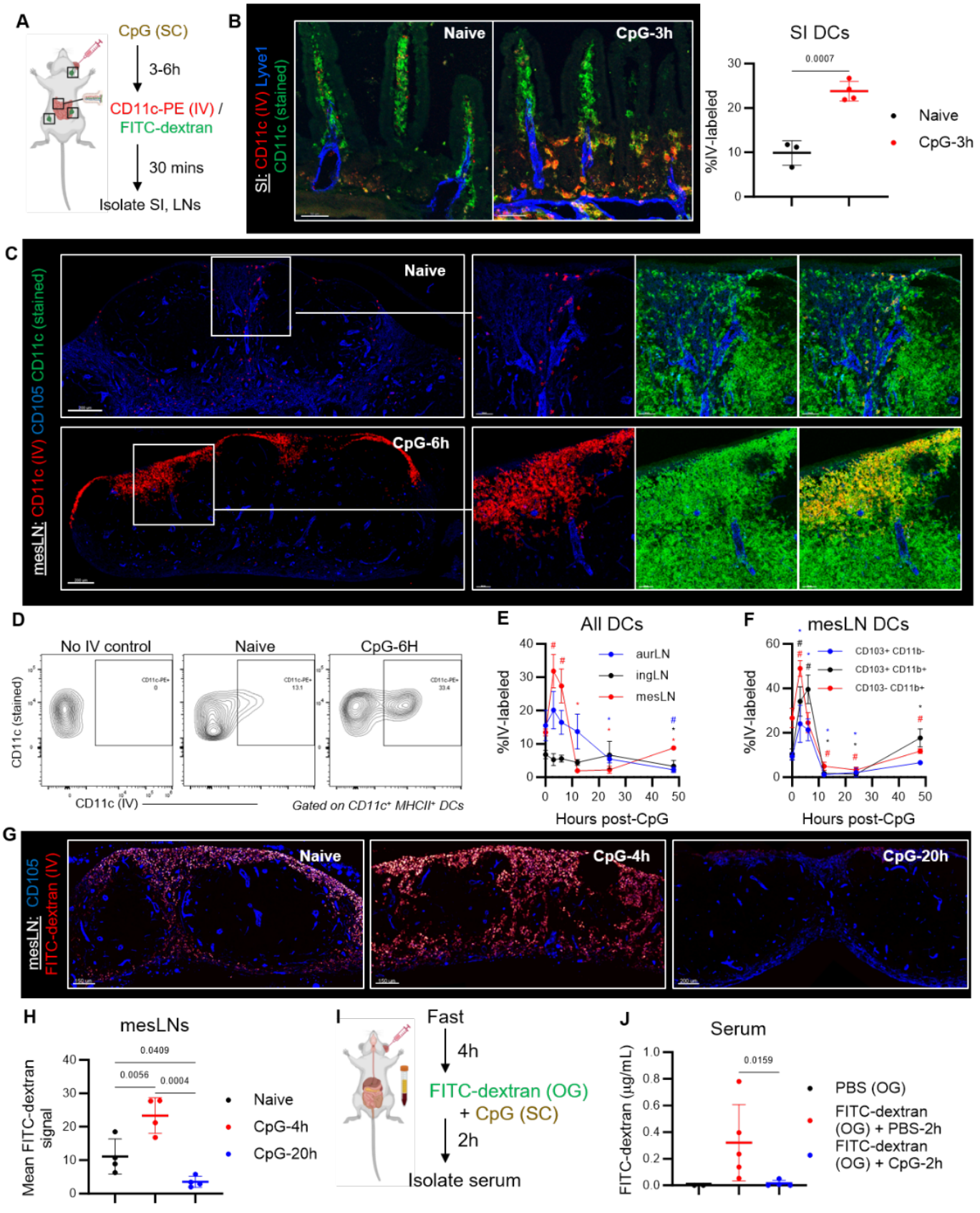

Figure 2. Enhanced endothelial permeability drives activation and intravenous labeling of intestinal DCs following cutaneous immunization. (A) C57BL6/J mice were injected in both ears with CpG for either 3 or 6h, or left untreated, followed by intravenous (IV) retro-orbital injection of CD11c-PE and/or 500 kD FITC-dextran. After 30 mins, the mice were euthanized, and LNs were harvested for analysis by microscopy or flow cytometry. **(B)** Representative images of IV-labeled DCs and Lyve1+ lymphatic vessels in SI villi 3h p.i. and quantification of IV-labeling frequency in CD11c^{+} MHC-II^{+} Imaris spot objects. Scale bars are 50 µm. (*n* = 3-4 mice). **(C)** Representative images showing IV-labeled cells in the SCS of mesLNs from naïve and CpG-

injected mice, as well as CD105$^+$ blood vessels. Scale bars are 200 μm (L) and 50 μm. **(D)** Representative flow plots showing IV-labeling in mesLN DCs 6h p.i. **(E)** Flow cytometry time course of DC IV-labeling in indicated LNs (*n* = 3-4 mice). **(F)** Flow cytometry time course of DC IV-labeling in distinct mesLN DC subsets (*n* = 3-4 mice) (*n* = 3-4 mice). **(G)** Representative images of FITC-dextran drainage in mesLN lymphatics 4 and 20h p.i. Scale bars are 150-200 μm. **(H)** Quantification of FITC-dextran signal in CD105$^+$ Imaris spot objects from (G) (*n* = 4 mice). **(I)** Diagram depicting study design for (J). C57BL6/J mice were fasted for 4h, after which they were orally gavaged (OG) with 10 mg of 4 kD FITC-dextran and injected in both ears with either PBS or CpG. 2h later, mice were euthanized and blood was isolated for analysis. **(J)** Quantification of serum FITC-dextran levels. Data are representative of at least two independent experiments (*n* = 2-5 mice). (A) was created on Biorender.com. Data in (E) and (F) were analyzed via one-way ANOVA with Benjamini, Krieger, and Yekutieli correction for multiple comparisons. * = $P < 0.05$ and # = $P < 0.0001$ and show statistical significance between the indicated time point and the naïve control group. Data are representative of at least two independent experiments. (A) and (I) were created on Biorender.com.

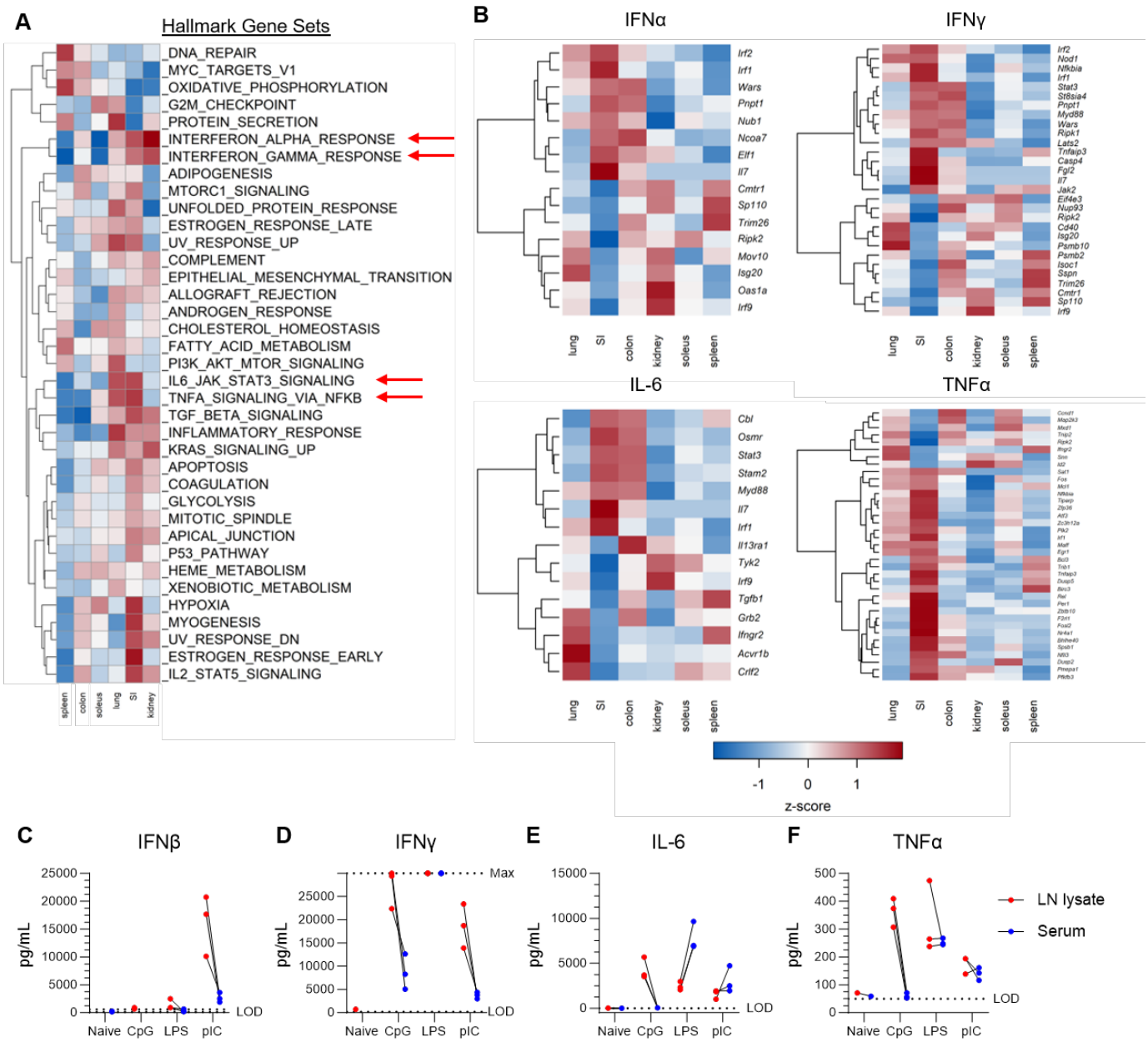

Figure 3. Molecular characterization of BECs and systemic cytokines. (A) Heatmap depicting differentially enriched MSigDB Hallmark gene sets across BEC populations from a published single-cell RNA sequencing data set (23) as analyzed by Gene Set Variant Analysis (GSVA). **(B)** Heatmaps depicting cytokine pathway genes which are differentially expressed in SI BECs compared to BECs in other tissues. **(C-F)** LEGENDplex screen for inflammatory cytokines in serum and draining LNs 6h after cutaneous adjuvant administration. Where appropriate, dotted lines indicate upper ("Max") and lower ("LOD") limits of detection respectively. Data in C are from a single experiment (*n* = 1-3 mice).

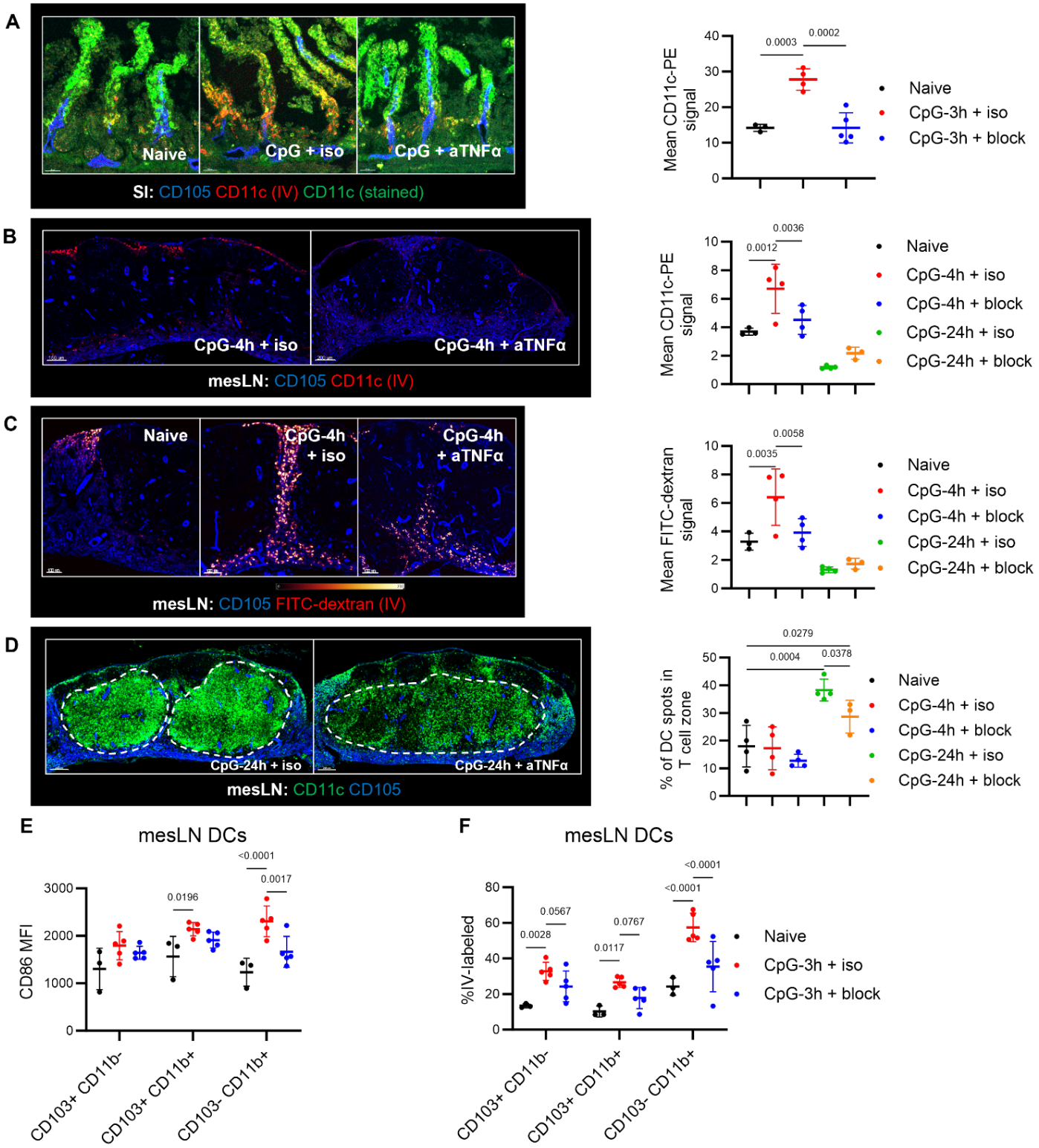

Figure 4. The intestinal alert state during distal inflammation is mediated by TNFα signaling.

(A) C57BL6/J mice were injected intraperitoneally with either anti-TNFα blocking antibody or isotype control. 1h later, they were injected in both ears with CpG for 3-24h or left untreated, followed by IV injection of CD11c-PE or 500 kD FITC-dextran. After 30 mins, SI and mesLNs were harvested for analysis. Representative microscopy images of IV-labeled DCs in SI villi 3h p.i. +/- TNFα blockade, and quantification of CD11c-PE intensity. Scale bars are 50 μm (*n* = 3-4 mice). **(B)** Representative images of IV-labeled DCs in mesLNs 4h p.i., +/- TNFα blockade, and quantification of CD11c-PE staining 4h and 24h p.i. Scale bars are 150-200 μm (*n* = 3-4 mice). **(C)** Representative images of FITC-dextran drainage to mesLN lymphatics 4h p.i. +/- TNFα blockade, and quantification of FITC-dextran intensity in CD105+ Imaris spot objects 4h and

24h p.i. Scale bars are 100 μm (*n* = 3-4 mice). **(D)** Representative images of mesLN DC repositioning into the T cell zone 24h p.i. +/- TNFα blockade, and quantification of this repositioning 4h and 24h p.i. White dashes denote the T cell zone boundary (*n* = 3-4 mice). **(E-F)** Quantification of CD86 exprssion (E) and IV-labeling (F) on mesLN DC subsets 3h p.i. +/- TNFα blockade. Data are representative of at least two independent experiments. Scale bars are 200 μm (*n* = 3-5 mice).

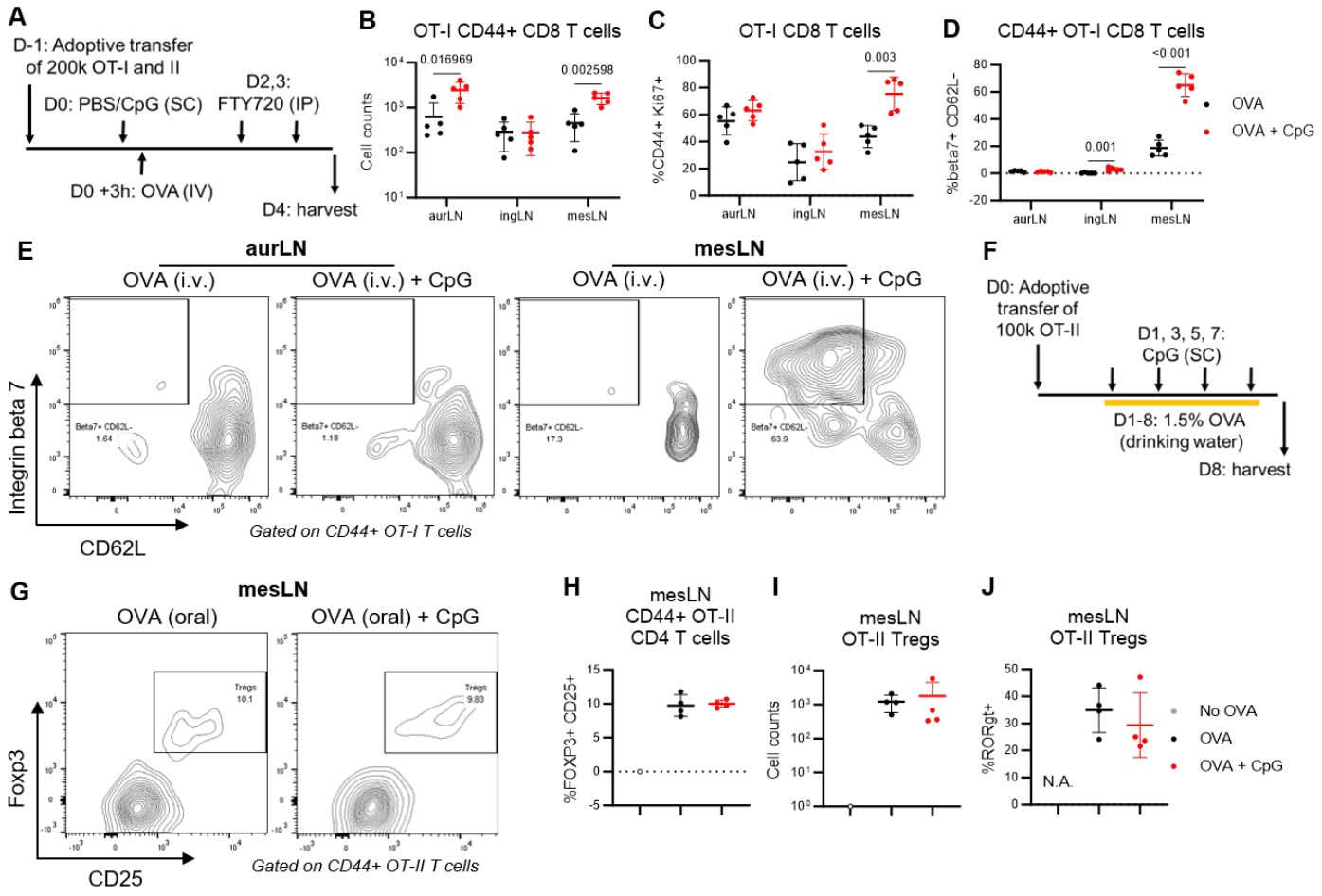

Figure 5. Cutaneous immunization potentiates adaptive immune responses to systemic antigens in mesLNs. (A) Diagram depicting study design for (B-E). 200,000 OT-I and OT-II (each) were adoptively transferred into C57BL6/J mice. One day later, recipients were injected in both ears with CpG for 3h or left untreated, followed by IV injection of 10 µg of OVA. Mice also received intraperitoneal FTY720 2 and 3 days later and were euthanized 4 days p.i. for analysis by flow cytometry. **(B)** Quantification of CD44$^+$ OT-I cell counts across indicated LNs (*n* = 5 mice). **(C)** Quantification of the CD44+ Ki67+ subset in OT-I T cells (*n* = 5 mice). **(D-E)** Quantification (D) and representative flow plots (E) of integrin β7 (beta7) and CD62L expression in CD44$^+$ OT-I cells across indicated LNs (*n* = 5 mice). **(F)** Diagram depicting study design for (G-H). Mice were adoptively transferred with 100,000 OT-II T cells and then fed OVA in drinking water for a week. Some animals also received CpG injections every other day, after which mesLNs were isolated for analysis by flow cytometry. **(G)** Representative flow plots of FOXP3 and CD25 expression on mesLN CD44$^+$ OT-II T cells. **(H-J)** Quantification of frequency (H), cellularity (I), and RORγt (J) expression on FOXP3$^+$ CD25$^+$ Tregs in mesLNs. Data are representative of at least two independent experiments (*n* = 1-4 mice).